IRIS AperTO

UNIVERSITÀ DEGLI STUDI DI TORINO

AperTO - Archivio Istituzionale Open Access dell'Università di Torino

Spontaneous aggregation of humic acid observed with AFM at different pH

This is the author's manuscript

Original Citation:

Availability:

This version is available http://hdl.handle.net/2318/1731486 since 2020-02-26T17:44:08Z

Published version:

DOI:10.1016/j.chemosphere.2015.08.010

Terms of use:

Open Access

Anyone can freely access the full text of works made available as "Open Access". Works made available under a Creative Commons license can be used according to the terms and conditions of said license. Use of all other works requires consent of the right holder (author or publisher) if not exempted from copyright protection by the applicable law.

(Article begins on next page)

12 October 2024

Atomic force microscopy for studying molecular dynamics in humic acid aggregates formed at different pH values

Claudio Colombo[a], Giuseppe Palumbo[a], Ruggero Angelico[a], Ornella Francioso[b], Andrea Ertani[c], Serenella Nardi[c]

[a]Dipartimento Agricoltura Ambiente Alimenti (DAAA), Università del Molise, Via De Sanctis 86100, Campobasso (CB), Italy

[b]Dipartimento di Scienze Agrarie (DipSA), Università di Bologna, V.le Fanin 40 40127, Bologna, Italy

[c]Dipartimento di Agronomia Animali Alimenti Risorse Naturali e Ambiente - DAFNAE

Viale dell'Università 16 – Agripolis 5020 Legnaro – Italy

*Corresponding author:

Abstract[1]

Atomic force microscopy (AFM) in contact (AFM-C) and non-contact (AFM-NC) modes was used to investigate the molecular dynamics of leonardite humic acid (HA) structures formed at different pH values. Individual or aggregate HA nanoparticles formed at pH values ranging from 2 to 12 were observed on a mica surface under dry conditions. The most clearly resolved and well-ordered AFM images were obtained in the AFM-C mode of aggregates formed at pH 5, where HA appeared as ring-shaped particles with a conic shape and a hole in the centre. These observations suggested that HA formed under these conditions exhibits a pseudo-amphiphilic nature, forming a ring structure with a polar head covering the mica and a hydrophobic tail in the centre of the micelles. Based on molecular simulation methods, a model lignin-carbohydrate complex (LCC) was proposed to explain the HA ring morphology. The model optimized the parameters of β-

[1] **Abbreviations:** AFM, atomic force microscopy; AFM-C, AFM in contact mode; AFM-NC, AFM non-contact mode; HA, humic acid; LCC, lignin-carbohydrate complex.

O-4 linkages between 14 units of 1-4 phenyl propanoid, and resulted in an optimized a structure comprising 45–50 linear helical molecules looped spirally around a central cavity.

Keywords: Humic acid, molecular conformation, atomic force microscopy.

1. Introduction

Chemical and physicochemical behaviour shown by humic acid (HA) in natural soil and water environments is a function of its molecular structure, and dictates its organic matter mobility, interaction with clay surfaces, and aggregation (Stevenson, 1994; Swift, 1989). HA has been described as a polyelectrolytic macromolecule of flexible molecular weight (Chen and Schnitzer, 1976; Hayes and Clapp, 2001), or as randomly polydispersed planar disks that form fairly compact soft spheroids (Duval et al., 2005; Schulten, 1999; Swift, 1999). In both conceptual models, the size, shape, and charge of HA molecules can change depending on solution pH and ionic strength (Alvarez-Puebla and Garrido, 2005; Borisover et al., 2001; Graber and Borisover, 1998).

A micellar model of HA was proposed by Wershaw (1986) in which micelles spontaneously aggregate, held together by weak forces such as hydrogen bonding, π-bonding, and charge transfer complexation. Micelles may be disaggregated or dispersed into smaller aggregates as a function of added organic acid concentration and pH (Piccolo et al. 1996; Wershaw, 1999). An important implication of this observation is that the most desirable soil structures may be formed through self-assembly or micellization and disaggregation. In nature, soil structure formation from minerals and organic particles by these processes is very common (Chin et al., 1998).

As in the micellar theory, the humic supramolecular association model proposed by Piccolo (2001) suggests that HA is an aggregation of relatively small molecules held together by weak dispersive forces instead of covalent linkages. Hydrophobic forces (e.g., van der Waals, π-π, and CH-π interactions) and hydrogen bonds are responsible for the apparent large molecular size of HA, the former becoming more important with increasing pH.

Shevchenko et al. (1999) simulated the molecular conformation of natural organic matter based on an oxidized lignin-carbohydrate complex (LCC) in which the parameters of the β-O-4 linkages in the oligomeric chain were optimized. The LCC can form on clay surfaces, and forms a molecular conformation using intertwined linear helical macromolecules.

Despite much research being carried out over the last decade, the details of HA conformation have still not been fully understood. While its main molecular building blocks have long been identified (Schulten and Leinweber, 2000), little is known about how these building blocks are linked and how they influence the molecular conformation.

Since the last 15 years, atomic force microscopy (AFM) is being used to observe the micromorphology of organic molecules and HA in aqueous and dry conditions (Eggleston et al., 1998; Maurice, 1996). Compared with electron microscopy techniques such as TEM and SEM, AFM has advantages in sample preparation, as there is no need for dehydration, coating, or high vacuum. This presents the possibility of probing the microstructure of organic and mineral colloids by surface analysis at different pH values and ionic strengths, and the results can be easily visualised as three-dimensional images (Liu et al., 2003; Maurice et al., 1999). Depending on HA concentration and pH, sponge-like structures, small disks (10–50 nm in diameter, 2–10 nm in height), aggregates of discs, chain-like assemblies, perforated sheets, and sponge-like ring structures have been observed in HA colloids using AFM (Balnois et al., 1999; Gorham et al., 2007). However, due to the complex nature of HA and the possibility of aggregation or conformational changes, the precise structure of HA remains uncertain. In addition, as reported by many researchers, determination of the molecular dynamics of HA by AFM measurements is difficult for several reasons concerning the geometry of, and force exerted by, the microscope tip, which can reduce the precision of the technique and increase the occurrence of error in the topographic data (Baalousha et al., 2005; Paredes et al., 2000).

In the present work, non-contact mode AFM (AFM-NC) and contact mode AFM (AFM-C) observations in air were compared in order to investigate HA conformation under different pH conditions. The description of the nanoscale 3D structure of HA as a function of pH is potentially useful in understanding HA interactions and building a more realistic model of HA structure and soil surfaces.

2. Materials and methods

2.1 Preparation of humic acid

Commercial humic acid (leonardite CIFO Humic from North Dakota) was used in our study, and was purified according to a procedure endorsed by the International Humic Substance Society. For further details concerning purification and characterisation of HA, see Colombo et al. (2012). Following this purification, a stock solution of 200 mg L^{-1} HA in the form of sodium humate was dialyzed with molecular weight cut-offs of 5000 and 10000 Da. For the AFM study of size variation as a function of pH, a suspension was diluted to 0.1 ± 0.0005 g of HA per litre of MilliQ-Distilled water. The diluted suspension was sonicated for 30 min, and 50 mL aliquots were adjusted to the desired pH values by the addition of 0.10 M HCl or NaOH at 298 K.

2.2 Sample AFM preparation

All AFM images were obtained by depositing the HA suspension on mica after 5 days of dehydrating at room temperature. Natural muscovite (Plano, Wetzlar, Germany) is an ideal horizontal surface for shape and size measurement as it is possible to observe individual HA particles distributed as a monolayer on the mica surface. Mica squares (1 cm^2) were freshly cut and positioned on a glass sample slide in order to obtain a flat, smooth surface with a natural negative charge.

2.3 AFM settings

Particle size (diameter and height) was estimated by AFM using a Park System Corporation XE-150 microscope in contact (AFM-C) and non-contact (AFM-NC) modes. AFM-C was performed using a NSC36A cantilever and a wedge of silicon nitride tips with a nominal tip radius of 20 nm at a force constant of 0.12 N/m. The set point voltage was approximately 2.0 V, and integral and proportional gains were adjusted for a different scan rate at 0.50 Hz. The AFM-C images are a record of the error in the height measurement of the sample under constant force mode, and were used to analyse surface micromorphology (Colombo et al., 2012).

AFM-NC images were obtained using a PPP-NCHR probe with a nominal tip radius of 7 nm. The probes have a nominal force constant of 20–100 N/m, and oscillate at a frequency of 312 kHz. The AFM-NC images were collected at scan rate of 0.50 Hz and a scan number of 512. The set point voltage was approximately 2.0 V, and integral and proportional gains were adjusted for different scans at around 0.2 and 5 V, respectively.

Layer diameter and thickness analysis was performed on single particles at different scan areas (10 × 10 μm, 5 × 5 μm, 1 × 1 μm) on a perfectly horizontal surface. The vertical height data were digitally recorded in order to obtain surface topography and were also used to evaluate the particle dimensions. All results were obtained from the analysis of 300 different particles.

2.4 Particle size distribution

The images were analysed using XEI analysis software 1.8.0 (Park System Corporation). Elevations relative to the base-plane of the surface were obtained and processed to estimate the dimensions of individual particles, i.e., area, volume, and average height (see Figures S1.1 and S1.2; Ohnesorge and Binning, 1993). Section and convolution analyses of images were carried out in order to examine the effect of the pH on the configuration of the HA molecules adsorbed on mica.

2.5 Molecular modelling

Molecular modelling was carried out using the ChemBioDraw 11 Software package (Cambridge, 2012). ChemBio3D Ultra was used to design the model based on energy minimization calculations that included contributions from van der Waals and electrostatic terms. Its molecular mechanics algorithm was also used to model hydrogen bonding in the aggregates (Sein et al., 1999). In the present study, the convergence limit was set using a maximum acceptable hydrogen bonding gradient of 0.042 kJ, and the simulation was performed on the optimized structure in order to derive the most probable conformation.

3. Results and discussion

3.1 Observation by AFM-C and AFM-NC

Figure 1 shows simultaneous topography and deflection images of single and aggregated HA particles prepared at pH 2, 5, and 12. The HA sample prepared at pH 2 appears as macroaggregates formed by subunit particles ranging in size from 60 to 300 nm (average 163 nm) with several larger globular particles of size 400–800 nm. From the figure, it is clear that multiple HA species are stacked on top of each other, indicating a strong interaction among the adsorbed particles prepared at pH 2.

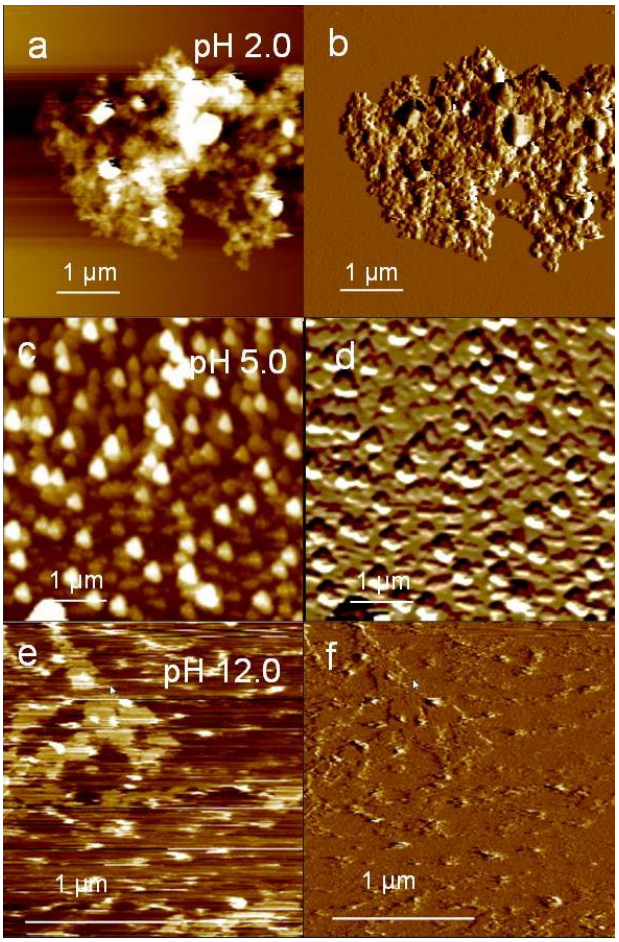

Figure 1. AFM-C images of HA aggregates. **(a)** Topography and **(b)** deflection of particles prepared at pH 2.0 (scan size: 5 × 5 µm, z range: 10 nm). **(c)** Topography and **(d)** deflection of particles prepared at pH 5.0 (scan size: 10 × 10 µm). **(e)** Topography and **(f)** deflection of particles prepared at pH 12.0 (scan size: 2 × 2 µm).

Angelico et al. (2014) used dynamic light scattering to investigate the kinetics of the flocculation process at pH 2, and reported that the apparent hydrodynamic diameter increased linearly with time from 800

to 1300 nm. At pH above 3, no aggregation phenomenon was observed and the humic particle diameter distribution was reported to be monodisperse. Also, Pédrot et al. (2010) reported similar observations on HA systems with an elevated aromatic nature. The reduction in the intermolecular electrostatic repulsion at pH 2 is responsible for the observed HA aggregation process (Alvarez-Puebla et al., 2006). It is noteworthy that our AFM observations of HA prepared at pH 2 revealed a large variation in particle thickness, i.e., the height in the z direction varied from 2 to 50 nm.

Aggregates formed at pH 5 showed well-dispersed conic single particles with a larger diameter of 260–280 nm and a height of 2 nm (±0.2 nm), as well as some clusters formed by 4–6 particles (Figures 1 (c) and (d)). Microtopographic AFM images of isolated HA particles dispersed at pH 5 (Figures 2 (a) and (b)) suggest that the cones are formed of smaller rings with interior pore spaces ranging from 20 to 30 nm. The topography section observed along the single red line (Figure 2 (b)) shows that the height of the peaks range from 4 to 6 nm, corresponding to 2–3 layers of the adsorbed HA. The margin of error in the height measurement by AFM is around 0.2 nm, and the roughness on the mica substrates used and the resolution of AFM in the z dimension is 0.05 nm or less.

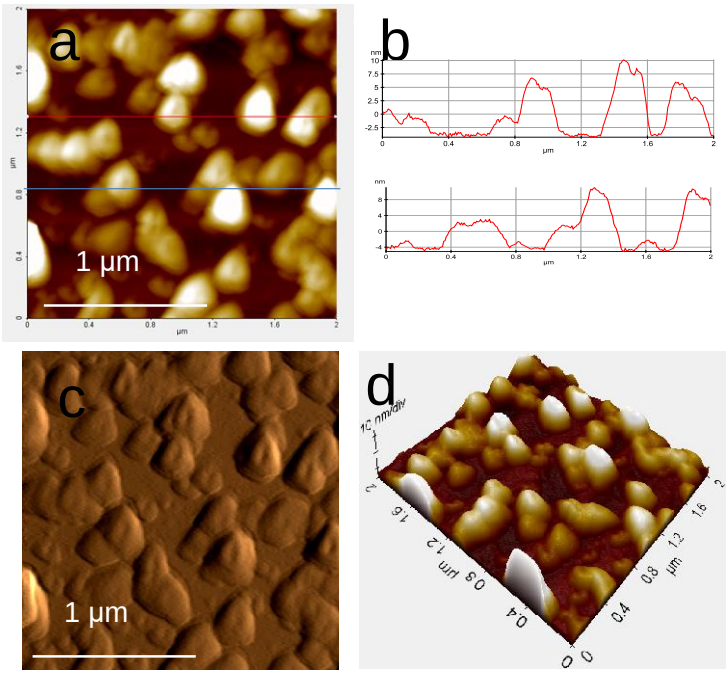

Figure 2. AFM-C images of isolated HA particles (scan size: 2 × 2 µm, z range: 10 nm). **(a)** Topographic, **(b)** line scan, **(c)** deflection, and **(d)** 3D projection images of isolated HA particles.

The HA particles prepared at pH 12 appear to be totally disaggregated and made up of a filamentous particles. They are disordered on the mica surface, and no vertical clustering is observed (Figures 1 (e) and (f)).

To better understand the HA particle shape, the microtopography observed with AFM-C was compared to that observed in the same sample with AFM-NC, as shown in Figure 3. In the AFM-NC measurement, the cantilever tip stays within the attractive force of the surface, reducing frictional influence on the HA, but lowering the resolution compared to that of AFM-C (Ohnesorge and Binning, 1993).

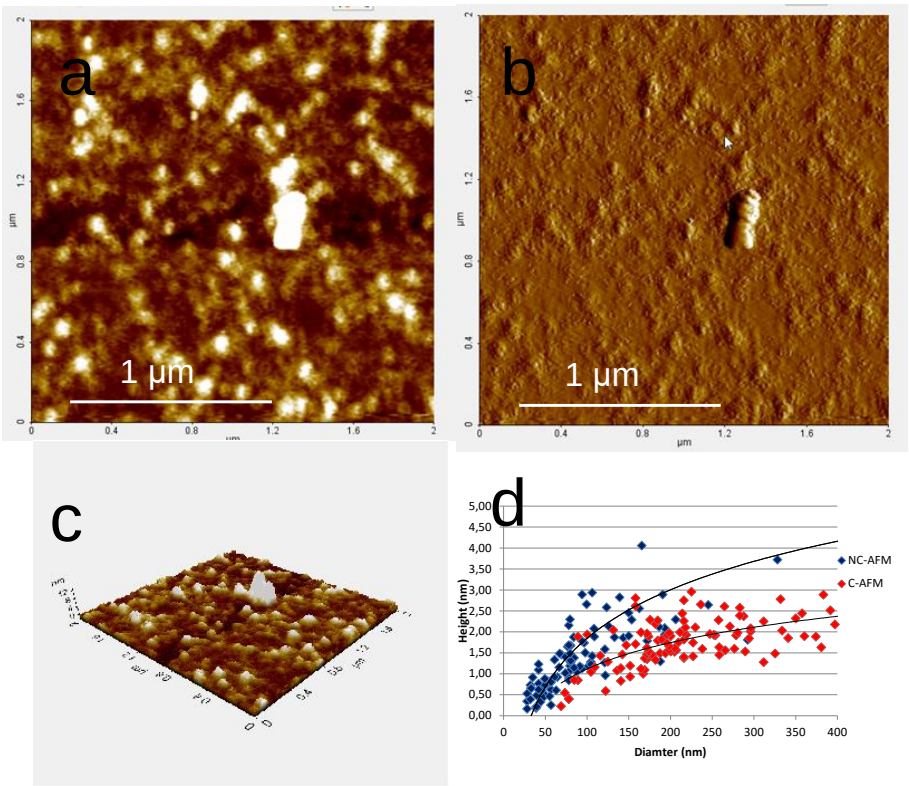

Figure 3. **(a)** AFM-NC (tapping mode) topography, **(b)** amplitude, and **(c)** 3D microtopography images of HA dispersed in pure water at pH 5 adsorbed and dried on a mica surface. **(d)** Diameters of individual HA particles observed with AFM-C and AFM-NC plotted vs. their measured heights.

AFM-NC topography and deflection images also show ring-shaped HA particles on the mica surface (Figures 3 (a) and (b)). The micromorphology of HA is different from that observed by AFM-NC, where HA or combined humic and fulvic fractions (HF) show generally better resolution (Chen et al., 2007). In Figure 3 (d), different measurements obtained with AFM-C (marked in red) and AFM-NC (marked in blue) are compared by plotting the diameters of the HA particles vs. their average heights as measured by each method. The particle size distribution obtained with AFM-CM demonstrates the presence of two kinds of particles: one in the range 50–200 nm (32%) and the second in the range 200–400 nm. When measured by AFM-NC, the average diameter of the particles is 264.65 nm and the average thickness is 1.22 nm; on the other hand, when measured by AFM-CM, the average diameter and thickness are 246.87 and 1.85 nm, respectively. This difference can be explained by the difference in the radius of curvature of the AFM-C and AFM-NC tips, which is related to significant broadening of features at the nanometer scale in the x-y plane (Baalousha et al., 2005).

3.2 Particle size distribution vs. pH observed with AFM-C

In Figure 4, the diameters of HA particles prepared at different pH values are plotted vs. their average heights, where every data point represents an individual particle. The HA prepared at pH 5 shows a large variation in particle diameter, with the distribution falling into two populations: one in the 50–200 nm range, and the other over 200 nm. Several single particles with 300–450 nm diameters and 3–4 nm heights are detected, arranged as clusters and horizontal aggregates. These relatively large variations in particle height at low pH reflect the height polydispersity of the HA molecules, which may be due to the presence of specific molecular surfaces that contribute at the formation of larger aggregates. Multiple adsorption layers are observed in many AFM images of HA prepared under acidic conditions; their presence is confirmed by bearing analysis, which shows that around 30% of the highest peaks in the height range are due to particle aggregation.

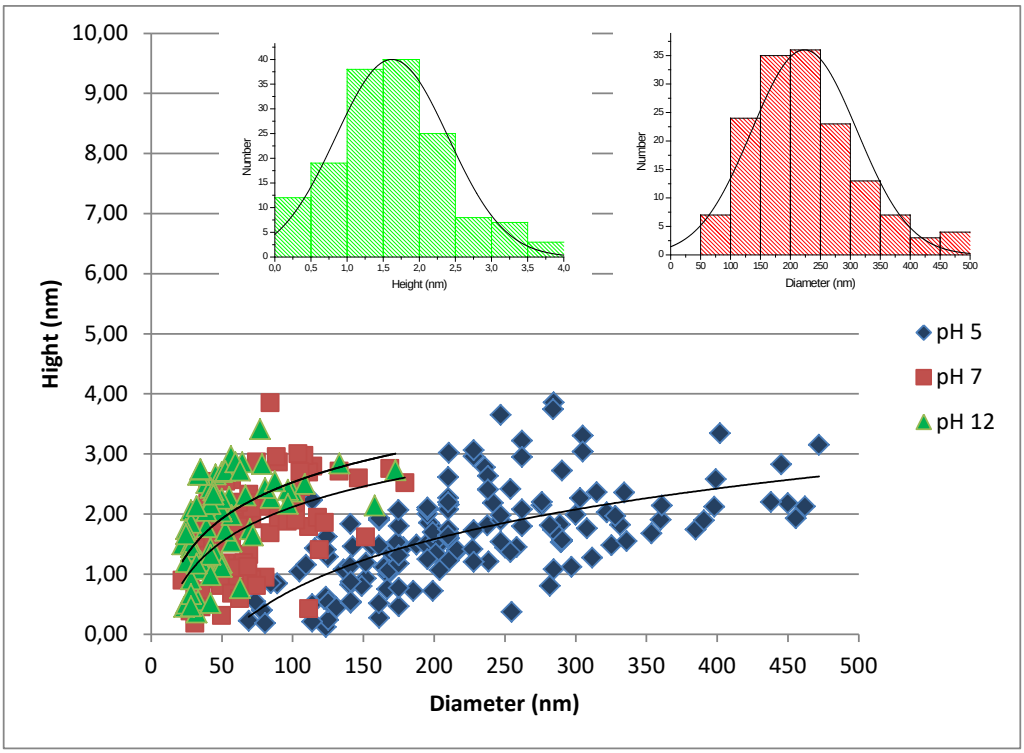

Figure 4. Diameter of individual HA particles prepared at pH 5, 7, and 12 vs. their heights, as measured by AFM-C. The insets show height (red) and diameter (green) population distributions for samples prepared at pH 5.

Considering the fact that 70% of the size population is confined to a narrow height range, we are confident that the height range from 1 to 2 nm in the water dried samples corresponds to the monolayer thickness of HA structures. The error margin of height measurement by AFM is about 0.2 nm or less. This estimate is based on the fact that the roughness of the mica substrates is 0.2 nm, and the ultimate resolution of the AFM in the z dimension is 0.1 nm or less.

The volumes of these ring-like structures ranged from 300 to 400 nm^3, as evaluated by image processing (see SI). Similar ring structures were also observed in the AFM tapping imaging of peat fulvic acid (Gorham et al., 2007; Liu et al., 2000; Maurice, 1998; Maurice et al., 1999; Namjesnik-Dejanovic and Maurice, 1997); AFM of liquid samples showed that HA existed as networks and torus-like structures (Plaschke et al., 1999). Liu et al. (2000) reported the HA particle thickness to be 0.6–4.4 nm for the spherical configuration and to be 0.19–2.5 nm for the ring-like configuration.

HA prepared at pH 7 produced particles with diameters below 200 nm and heights ranging from 1 to 4 nm, with several outer layers (Figure 4).

In the HA prepared at pH 12, only one particle type was observed, with average diameter dimension of 108 nm and thickness of 1–3 nm. The diameter of these particles increases linearly with increasing height in the range 0.5–3.5 nm, indicating that, globular structures are unstable in HA produced at this pH. As pH increases, the vertical association of the HA particles becomes less favourable, leading to a decrease in particle thickness. When dispersed in alkaline solution, the HA particles clearly become more open, showing significantly wider structures (Alvarez-Puebla and Garrido, 2005). At pH 12, it is reasonable to assume that the phenolic groups of HA, with pKa values between 4 and 5, are completely deprotonated, as are the carboxyl and hydroxyl groups, which have pKa values of ~9. The deprotonated carboxylic and hydroxyl groups of HA are known to be the principal source of the molecular surface negative charge. In addition, the most important binding sites are totally saturated by Na, increasing the dissociation of the functional groups of the HA molecule. Under these conditions, it is possible that the macromolecule charge of the HA particles decreases, leading to an increase in intra- and intermolecular repulsions, forcing a linear expansion of the colloids to minimize repulsive effects. This expansion likely leads to the disintegration of micelles that are generated during the aggregation processes.

3.3 Computational molecular models for HS molecule

Computational molecular models for HA, based on their chemical composition as determined by analytical measurements with NMR (see the SI), are shown in Figure 5 (a) and (b). The model LCC is formed from 14 1-4 phenyl propanoid units linked in linear chains, with 60% arylglycerol β aryl ether (β-O-4) linkages, 30% phenylcoumaran unit (β-5) linkages, and 20% 5-5 unit linkages optimizing the chain conformation as an irregular extended helix (Figure 5 (b)), giving a total chemical formula of $C_{128}H_{140}O_{37}$ and a molecular weight of 2270.46 g mol^{-1}. The helical structure of the LCC molecule is shown in Figure 5 (a). The computational molecular conformation of the LCC molecule was derived from *in vacuo* simulation, meaning that HA is modelled in the solid state and no other substances such as water are included in the system (Figure 5 (b)). These calculations aim to derive the most realistic, i.e., optimized, 3D geometrical

arrangement of the HA molecule by minimizing the potential energy of the system (Kalinichev, 2007; Sein et al., 1999).

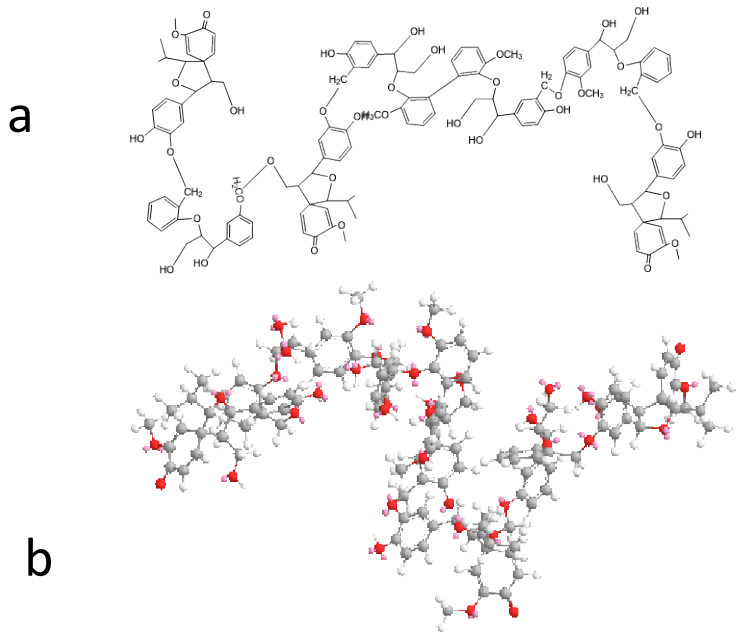

Figure 5. Helical conformation of HA derived from molecular simulation. **(a)** Chemical formula and **(b)** ball-and-stick representation.

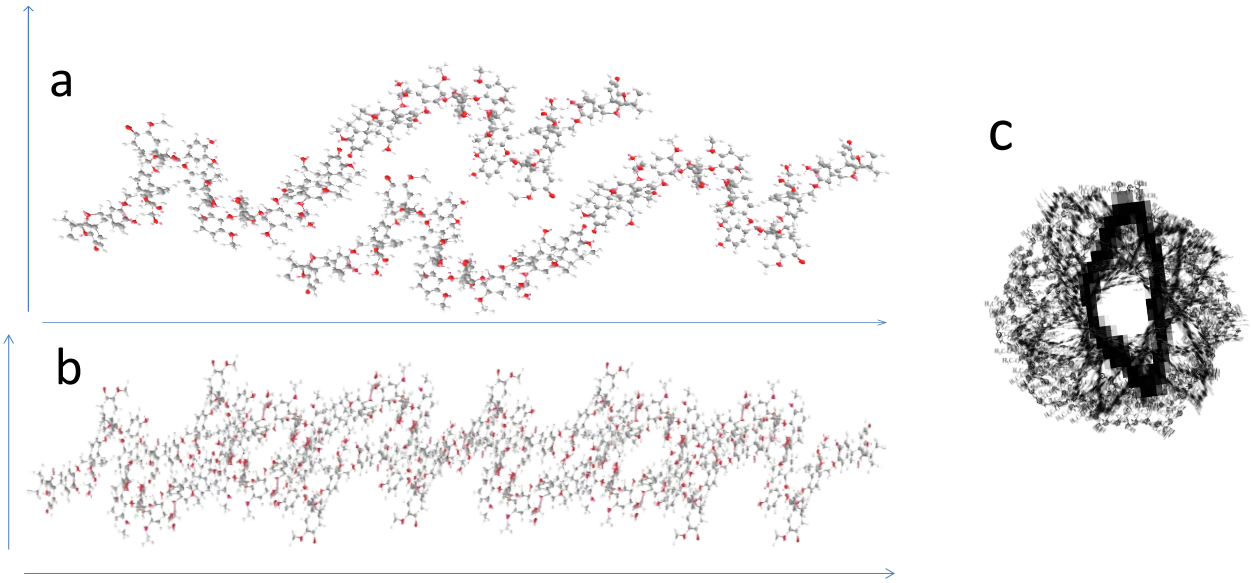

Figure 6. Molecular modelling results. **(a)** Overlapping helical structures formed by three subunits of the phenyl propanoid chain linked in a regular linear sequence. **(b)** Linear structure formed from two overlapped chains composed of six units. **(c)** 45–50 linear helix molecules looped spirally to form a ring.

The simulated LCC helix chains produced a molecular aggregate formed comprising 45–50 linear subunits looped spirally that produces ring structures with a cavity in the centre (Figure 6). Preferential formation of helixes for lignin chains and polymers of similar nature has been already reported (Rapaport, 2002). This makes it a particularly interesting model for the quantitative investigation of HA with molecular modelling techniques (Kawahigashi et al., 2005). The sodium ion charge of HA seems to play an important role in supporting the supramacromolecular structure (Au et al., 1999; Kalinichev and Kirkpatrick, 2007).

These HA structures are supported by previous AFM investigations of fluvic acid samples where ring-like structures or chain-like assemblies were observed (Balnois et al., 1999; Gorham et al., 2007; Lead et al., 2005; Liu et al., 2000; Maurice et al., 1999). Furthermore, in SEM and TEM studies, perforated sheet-like structures, longer chains, fibres, or bundle of fibres were observed (Chen and Schnitzer, 1976). This may be attributed to the fact that samples for electron microscopy are commonly prepared at much higher HA concentrations than used in this study, resulting in HA precipitations that occur when highly concentrated solutions are rapidly dried. During the drying procedure, changes in the chemical composition of the sample solution and the surface tension of droplets results in concentration gradients, and structures and may be influenced by shrinkage. Nevertheless, to better understand the role of HA in soil, it is necessary to thoroughly quantify its conformation, and, subsequently, to determine the binding mechanisms in an analogous manner to the function relationships in biological macromolecules (Muscolo et al., 2007).

5. Conclusions

The structures of HA aggregates adsorbed on mica observed in AFM micrographs show a considerable dependence on the pH of the solutions used in the preparation of the aggregates. The aggregates prepared at pH 5 showed conic ring structures. In the absence of hydration forces and at acidic pH, the HA conformation is stabilized by intramolecular ð-ð and van der Waals interactions. A favourable interaction between the HA particle and the hydrophilic mica surface results in orientations that maximize the contact area at the solid/liquid interface. Based on molecular simulation methods, an LCC molecular model was proposed to explain the ring conformation of HA. The model optimized the parameters of β-O-4 linkages between 14 1-4

phenyl propanoid units in a simple oligomeric chain. The HA structure appeared to comprise 45–50 linear LCC helix molecules looped in a spiral around a central cavity. The LCC model provided a complete description of the 3D nano/microstructure of HA, depending on the pH employed in its preparation.

These results are very helpful for understanding the influence of carboxylic and phenolic group ionization on the HA molecular arrangement in terms of size, strength, and flexibility. Covalent and hydrogen bonds appear to stabilize the helical structure, while van der Waals interactions hold the oligomeric chain. The proposed model is a significant step towards a full understanding of soil HA structure and function.

Acknowledgments

We thank Prof. Hyengoo Cho of the Gyeongsang National University, Jinju, Republic of Korea, for providing access to his AFM system and for help with molecular modelling, and Prof. Alessandro Piccolo for assistance with NMR determination. Financial support from the Consorzio per lo sviluppo dei Sistemi a Grande Interfase (CSGI) is gratefully acknowledged.

Supporting Information Available: Additional details of the AFM set up and data processing are described.

References

Alvarez-Puebla, R.A., Garrido, J., 2005 Effect of pH on the aggregation of a gray humic acid in colloidal and solid states. Chemosphere 59, 659–667.

Alvarez-Puebla, R.A., Valenzuela-Calahorro, C., Garrido, J., 2006. Theoretical study on fulvic acid structure, conformation and aggregation: a molecular modelling approach. Sci. Total Environ. 358, 243–254.

Angelico, R., Ceglie, A., Ji-Zheng, H., Yu-Rong, L., Palumbo, G., Colombo, C., 2014. Particle size, charge and colloidal stability of humic acids coprecipitated with ferrihydrite. Chemosphere 99, 239-247.

Au, K.K., Penisson, A.C., Shuolin, Y., O'Melia, C.R., 1999. Natural organic matter at oxide/water interfaces: complexation and conformation. Geochim. Cosmochim. Acta 63, 2903–2917.

Balnois, E., Wilkinson, K.J., Lead, J.R., Buffle, J., 1999. Atomic force microscopy of humic substances: effects of pH and ionic strength. Environ. Sci. Technol. 33, 3911–3917.

Baalousha, M., Motelica-Heino, M., Galaup, S., Coustumer, P., 2005. Supramolecular structure of humic acids by TEM with improved sample preparation and staining. Microsc. Res. Tech. 66, 299−306.

Borisover, M., Reddy, M., Graber, E.R., 2001. Solvation effect on organic compound interactions in soil organic matter. Environ. Sci. Technol. 35, 2518–2524.

Chin, W.C., Orellana, M.V., Verdugo, P., 1998. Spontaneous assembly of marine dissolved organic matter in polymer gels. Nature 391, 568–571.

Chen, C.L., Wang, X.K., Jiang, H.W.P., Hu, W.P., 2007. Direct observation of macromolecular structures of humic acid by AFM and SEM. Colloid Surface A 302, 121–125.

Chen, Y., Schnitzer M., 1976. Scanning electron microscopy of a humic acid and its metal and clay complexes. Soil Sci. Soc. Am. J. 40, 682–686.

Colombo, C., Palumbo, G., Sellitto, V.M., Rizzardo, C., Tomasi, N., Pinton, R., Cesco, S., 2012. Characteristics of insoluble, high molecular weight iron-humic substances used as plant iron sources. Soil Sci. Soc. Am. J. 76, 1246–1256.

Kalinichev, A.R.J., Kirkpatrick, R.J., 2007. Molecular dynamics simulation of cationic complexation with natural organic matter. Eur. J. Soil Sci. 58, 909–917.

Kawahigashi, M., Sumida, H., Yamamoto, K., 2005. Size and shape of soil humic acids estimated by viscosity and molecular weight. J Colloid Interf. Sci. 284, 463–469.

Duval, J.F.L., Wilkinson, K.J., van Leeuwen, H.L., Buffle, J., 2005. Humic substances are soft and permeable: evidence from their electrophoretic mobilities. Environ. Sci. Technol. 39, 6435–6445.

Eggleston, C.M., Higgins, S.R., Maurice, P.A., 1998. Scanning probe microscopy of environmental interfaces. Environ. Sci. Technol. 32, 456–459.

Hayes, M.H.B., Clapp, C.E., 2001. Humic substances: Considerations of compositions, aspects of structure, and environmental influences. Soil Sci. 166, 723–737.

Graber, E.R., Borisover, M.D., 1998. Hydration-facilitated sorption of specifically-interacting compounds by model soil organic matter. Environ. Sci. Technol. 32, 258–263.

Gorham, J.M, Wnuk, J.D., Shin, M., Fairbrother, H., 2007. Adsorption of natural organic matter onto carbonaceous surfaces: atomic force microscopy study. Environ. Sci. Technol. 41, 1238–1244.

Lead, J.R., Muirhea, A., Gibson, C.T., 2005. Characterization of freshwater natural aquatic colloids by atomic force microscopy. Environ. Sci. Technol. 39, 6930–6936.

Liu, A.G., Wu, R.C., Eschenazi, E., Papadopoulos, K., 2000. AFM on humic acid adsorption on mica. Colloids Surface A 174, 245–252.

Liu, C., Li, X., Xu, F., Huang, P.M., 2003. Atomic force microscopy of soil inorganic colloids. Soil Sci. Plant Nutr. 49, 17–23.

Maurice, P.A., 1996. Applications of atomic force microscopy in environmental colloid and surface chemistry. Colloids Surface 107, 57–75.

Maurice, P.A., Namjesnik-Dejanovic, K., 1999. Aggregate structures of sorbed humic substances observed in aqueous solution. Environ. Sci. Technol. 33, 1538–1541.

Namjesnik-Dejanovic, K., Maurice, P.A., 1997. Atomic force microscopy of soil and stream fulvic acids. Colloids Surface A 120, 77–86.

Ohnesorge, F., Binning, G., 1993. True atomic resolution by atomic force microscopy through repulsive and attractive forces. Science 260, 1451–1456.

Pédrot, M., Dia, A., Davranche, M., 2010. Dynamic structure of humic substances: rare earth elements as a fingerprint. J. Colloid Interf. Sci. 345, 206–213.

Paredes, J.I., Martià, A., Nez-Alonzo, J.M.D., Tascoà, N., 2000. Adhesion artefacts in atomic force microscopy imaging J. Microsc. 200, 109–113.

Piccolo, A., Nardi, S., Concheri, G., 1996. Macromolecular changes of soil humic substances induced by interactions with organic acids. Eur. J. Soil Sci. 47, 319–328.

Piccolo, A. 2001. The supramolecular structure of humic substances. Soil Sci. 166, 810–832.

Plaschke, M., Römer, J., Klenze R., Kim J.I., 1999. In situ AFM study of sorbed humic acid colloids at different pH. Colloids Surfaces A 160, 269–279.

Rapaport, D.C., 2002. Molecular dynamics simulation of polymer helix formation using rigid-link methods. Phys. Rev E 66, 011906.

Shevchenko, S.M., Bailey, G.W., Akim, L.G., 1999. The conformational dynamics of humic polyanions in model organic and organo-mineral aggregates. J. Mol. Struct. 460, 179–190.

Schulten, H.R., 1999. Analytical pyrolysis and computational chemistry of aquatic humic substances and dissolved organic matter. J Anal. Appl. Pyrol. 49, 385–415.

Schulten, H.R., Leinweber, P., 2000. New insights into organic mineral particles: composition, properties, and models of molecular structure. Biol. Fertil. Soils 30, 399–432.

Sein, L.T., Varnum, J.M., Jansen, S.A., 1999. Conformational modeling of a new building block of humic acid approaches to the lowest energy conformer. Environ. Sci. Technol. 33, 546–552.

Stevenson, F.J., 1994. Humus Chemistry: Genesis, Composition, Reactions. Wiley, Hoboken.

Swift, R.S., 1989. Molecular weight, size, shape and charge characteristics of humic substances: some basic considerations, in: Hayes, M.H.B., MacCarthy, P., Malcolm, R.L., Swift, R.S. (Eds.), Humic Substances II. In Search of Structure. Wiley, New York, pp. 449–466.

Swift, R.S., 1999. Macromolecular properties of soil humic substances: fact, fiction, and opinion. Soil Sci. 164, 790–802.

Sutton, R., Sposito, G., 2005. Molecular structure in soil humic substances: the new view. Environ. Sci. Technol. 39, 9009–9015.

Wershaw, R.L., 1986. A new model for humic materials and their interactions with hydrophobic organic chemicals in soil-water or sediment-water systems. J. Contam. Hydrol. 1, 29–45.

Wershaw, R L., 1999. Molecular aggregation of humic substances. Soil Sci. 164, 803–813.